Robust Avoidance of Edge-Localized Modes alongside Gradient Formation in the Negative Triangularity Tokamak Edge

A. O. Nelson, L. Schmitz, C. Paz-Soldan, K. E. Thome, T. B. Cote, N. Leuthold, F. Scotti, M. E. Austin, A. Hyatt, and T. Osborne

Phys. Rev. Lett. **131**, 195101 — Published 8 November 2023

DOI: 10.1103/PhysRevLett.131.195101

Robust avoidance of edge-localized modes alongside gradient formation in the negative triangularity tokamak edge

A. O. Nelson,[1] L. Schmitz,[2] C. Paz-Soldan,[1] K. E. Thome,[3] T. B. Cote,[3]
N. Leuthold,[1] F. Scotti,[4] M. E. Austin,[5] A. Hyatt,[3] and T. Osborne[3]

[1] *Columbia University, New York, NY 10027, USA*
[2] *University of California – Los Angeles, Los Angeles, CA 90095, USA*
[3] *General Atomics, San Diego, California 92186, USA*
[4] *Lawrence Livermore National Laboratory, Livermore, CA, USA*
[5] *The University of Texas at Austin, Austin, Texas 78712, USA*

(Dated: September 21, 2023)

In a series of high performance diverted discharges on DIII-D, we demonstrate that strong negative triangularity (NT) shaping robustly suppresses all edge-localized mode (ELM) activity over a wide range of plasma conditions: $\langle n \rangle = 0.1 - 1.5 \times 10^{20}\,\mathrm{m}^{-3}$, $P_{\mathrm{aux}} = 0 - 15\,\mathrm{MW}$ and $|B_{\mathrm{t}}| = 1 - 2.2\,\mathrm{T}$, corresponding to $P_{\mathrm{loss}}/P_{\mathrm{LH08}} \sim 8$. The full dataset is consistent with the theoretical prediction that magnetic shear in the NT edge inhibits access to ELMing H-mode regimes; all experimental pressure profiles are found to be at or below the infinite-n ballooning stability limit. Our present dataset also features edge pressure gradients in strong NT that are closer to an H–mode than a typical L-mode plasma, supporting the consideration of NT for reactor design.

Magnetic fusion energy reactors must achieve significant plasma pressures alongside sufficiently high energy confinement times in order to achieve the high fusion gain ($Q \sim 20 - 30$) needed for net energy production. The predominant approach employed to meet these requirements involves tokamak operation in a high-confinement (H-mode) scenario with positive triangularity (PT), which features a region of steep pressure gradients near the plasma edge called the pedestal [1]. While strong pedestals raise the core plasma pressure, they also beget violent instabilities called edge-localized modes (ELMs) that periodically connect the hot core plasma to the cooler edge region and deposit tremendous heat fluxes on the machine wall [2, 3]. In a reactor, it is expected that ELMs will be powerful enough to cause significant and potentially fatal damage to plasma-facing components [4], necessitating development of a reactor scenario that operates at high performance while simultaneously remaining completely ELM-free [5].

Numerous ELM avoidance strategies have been pursued as potential solutions to this power-handling problem. These include quiescent H-mode (QH-mode) [6], ELM suppression with resonant magnetic perturbations (RMPs) [7], the quasi-continuous exhaust (QCE) regime [8], improved-confinement (I-mode) [9], highly radiative low-confinement (L-mode) [10] and enhanced D_{alpha} H-mode [11], among others. Each of these techniques achieves ELM suppression through the introduction of an additional transport-inducing process in the plasma edge that prevents access to standard ELMing H-mode operation, often at some (manageable) expense in overall plasma performance. While it is hoped that some of these techniques will be applicable during high performance plasma operation on machines like ITER, they are each subject to different access criteria that are difficult to robustly extrapolate towards reactors [5, 12].

Recently, extensive work on the TCV [13–15], DIII-D [16, 17] and AUG [18] tokamaks has renewed interest in an alternative ELM-avoidance strategy involving operation with negative triangularly (NT) shaping [19]. The plasma triangularity (δ) is defined as the average of the upper and lower triangularities $\delta_{\mathrm{u},\ell} \equiv (R_{\mathrm{geo}} - R_{\mathrm{u},\ell})/a_{\mathrm{minor}}$, where R_{geo} is the geometric major radius, $R_{\mathrm{u},\ell}$ are respectively the major radius of the highest and lowest points along the plasma separatrix, and a_{minor} is the minor radius of the plasma. Early experiments in this regime [13, 14, 16, 17] have been able to achieve strong core performance (confinement factors [20] of $H_{98\mathrm{y2}} > 1$ and normalized pressures of $\beta_{\mathrm{N}} > 2.5$) but do not enter ELMing H-mode beyond a critical average triangularity $\delta < \delta_{\mathrm{crit}}$, optimistically indicating that NT shaping could offer a solution to the power-handling problem faced by tokamak plasmas and relax constraints on the auxiliary heating systems for reactors [21, 22].

In this Letter, we comprehensively analyze new data from a high-power NT campaign on the DIII-D tokamak to demonstrate that robust ELM and H-mode avoidance are fundamental properties of the NT edge and that it does not inhibit access to high core pressure. A unique set of carbon plasma-facing components is installed in the DIII-D tokamak that allows for strongly-shaped, diverted NT operation at record heating powers and densities [23]. Throughout this new dataset, $\delta < \delta_{\mathrm{crit}}$ robustly prevents ELMs, as the inherent nature of these NT plasmas is not to enter H-mode. A particular class of magnetohydrodynamic (MHD) instability, the ideal ballooning mode, is identified as a fundamental gradient-limiting mechanism in the NT edge that allows for pedestal formation while avoiding the instability limits responsible for triggering ELMs, confirming theoretical predictions from previous work [24]. The analysis presented here indicates that the NT edge is fundamentally different from standard L-

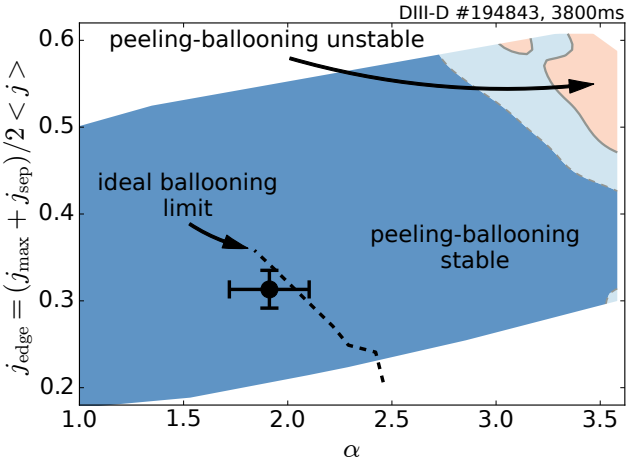

FIG. 1: Calculation of the infinite-n ballooning (dashed line) and peeling-ballooning (blue-red) limits for a typical high-performance NT plasma on DIII-D.

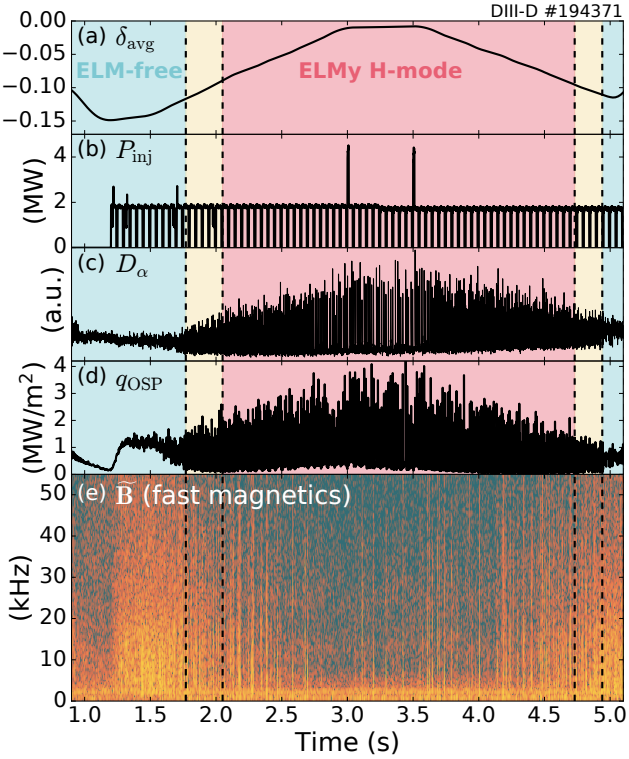

FIG. 2: As the triangularity (a) is varied at constant input power (b), the plasma transitions smoothly from an ELM-free state (blue) to an ELMing H-mode regime (red) through a oscillatory transition (yellow). Measurements of the D_α line emission (c) and divertor heat flux (d) demonstrate that peak power incident on the machine walls is strongly reduced during operation at strong NT. (e) Inspection of high-frequency magnetic fluctuations during this time reveals enhanced turbulent activity during the ELM-suppressed periods.

mode plasmas in PT even at matched power, being able to access relatively high edge pressures. As such, we propose that it is more accurately described as an "NT edge" than as "L-mode."

The leading understanding of H-mode behavior identifies coupled, finite-n peeling-ballooning (PB) modes as the fundamental MHD instability responsible for triggering ELMs in the plasma edge [3]. Peeling-ballooning instabilities are destabilized both by strong edge current (j_{edge}) and by strong normalized pressure gradients (α), thereby setting a hard upper limit on the conditions achievable in the plasma edge. Here α is defined as

$$\alpha = \frac{\mu_0}{2\pi^2}\frac{\partial V}{\partial \psi}\left(\frac{V}{2\pi^2 R_0}\right)^{1/2}\frac{dp}{d\psi}, \qquad (1)$$

where V is the volume enclosed by each flux surface, ψ the poloidal flux, p the plasma pressure and R_0 the plasma major radius. To avoid triggering ELMs, additional edge transport must be induced in order to ensure that j_{edge} and α are held some distance below the PB limit. This is achieved, for example, through the edge harmonic oscillation (EHO) in QH-mode plasmas [6], magnetic island chains in plasmas with RMP [25] and the weakly coherent mode (WCM) in I-mode [9].

In NT plasmas, the ideal (infinite-n) ballooning mode has been proposed as the ultimate gradient-limiting mode responsible for ensuring that the PB instability is not reached [24, 26]. As described in reference [24], the local magnetic shear s has a peak near the separatrix x-points for tokamak plasmas and a minimum on the outboard midplane. Notably, the shear stabilization for ballooning modes is proportional to s^2 [27]. In NT, the x-points are radially farther from the machine center than the equilibrium magnetic axis, localizing the maximum in s to the destabilizing "bad curvature" region of the plasma. This means that NT geometries force a null-crossing in s to appear in the bad curvature edge region, which destabilizes ideal ballooning modes at the so-called "1^{st} stability limit" [19, 24]. In conventional PT geometries, these modes are stabilized throughout the entire bad curvature region, opening a window to a 2^{nd} stability region that supports gradient growth typical of an H-mode pedestal. For a typical high-performance NT plasma on DIII-D with $\delta \sim -0.5$, the ideal ballooning and PB limits are calculated using the MHD stability codes BALOO [28] and ELITE [29], respectively, and plotted in figure 1. Notably, the ideal ballooning limit appears at a lower α than the PB limit, preventing the triggering of ELMs by limiting edge gradient growth via the same mechanism as the QCE ballooning mode [30] and in a manner akin to the QH-mode EHO and I-mode WCM. Additionally, the existence of this gradient limit means that NT plasmas do not enter H-mode [19, 24, 26, 31]. In the context of reactor implementation, this implies that, unlike in PT, a certain level of power crossing the separatrix may not be needed to maintain good core confinement, thereby reducing the demands on the auxiliary heating systems. A further discussion of this feature of NT plasmas is in-

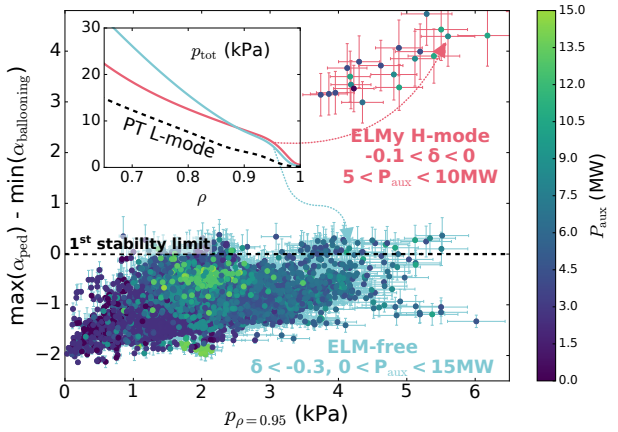

FIG. 3: Within experimental error bars, DIII-D discharges with strong NT ($\delta < -0.3$, blues) are limited by the 1^{st} ballooning stability limit. For comparison, a selection of ELMy H-modes with weaker δ and access to the 2^{nd} stability region are shown in red. Inset: profiles (all with $P_{aux} \sim 8\,MW$) are compared for representative NT ELM-free, weak NT H-mode and PT L-modes.

cluded in the appendix.

To demonstrate the sensitivity of NT ELM suppression on the plasma shape, in figure 2 the triangularity δ is varied in time at constant heating power ($P_{inj} \approx 2\,MW$). Small changes in δ near $\delta_{crit} \sim -0.12$ prompt smooth transitions from an ELM-free regime to an ELMy H-mode with slightly elevated β_N. In contrast to the expected behavior in PT plasmas, the transition between the ELM-free state and the ELMy H-mode state is not realized experimentally as an abrupt phase transition, but rather evolves smoothly through a transitional dithering phase [17] as the stability window is slowly widened. This is evidenced by the slowly evolving D_{alpha} emission measurement shown in figure 2(c). The evolution of the outer strikepoint heat flux (q_{OSP}, measured with infrared thermography) is plotted in figure 2(d). As compared to the ELMy H-mode phase, the ELM-free phases show (a) a decrease in the peak heat flux due to the absence of ELMs and (b) a corresponding increase in the steady-state heat flux as compared to the inter-ELM phases such that the time-averaged power remains the same. The absence of large transient heat fluxes supports the idea that NT configurations may ameliorate the power-handling problem presented by ELMs [4, 31–33]. Fourier analysis of high-frequency magnetic measurements shows strong broadband fluctuations in the ELM-free state when heating power is introduced (figure 2(e)), consistent with enhanced turbulence when the ballooning stability limit is reached. Notably, no strong hysteresis effect is observed when entering or leaving the ELM-free state, consistent with physics dominated by ideal MHD activity.

Unlike the gradient-limiting mechanisms responsible for ELM suppression in other regimes, destabilization of the ideal ballooning mode is a direct consequence of the magnetic geometry and is thus entirely robust to changes in plasma conditions. To demonstrate the simplicity of this effect, we utilize recent developments in automatic kinetic equilibrium reconstructions [34] to visualize ideal ballooning stability on a dataset level. Over 7500 equilibrium reconstructions from 265 representative equilibria with $\delta < -0.3$ are analyzed and presented in figure 3. These data cover a wide range of plasma conditions spanning the new diverted NT dataset space on DIII-D, including heating powers from $0 < P_{aux} \lesssim 15\,MW$, volume-averaged densities of $\langle n \rangle = 0.1 - 1.5 \times 10^{20}\,m^{-3}$, applied torques of $T_{inj} = -4$ to $10\,N\text{-}m$, plasma currents of $0.3 < I_p < 1.1\,MA$, on-axis magnetic fields of $1 < |B_t| < 2.2\,T$, and both attached and detached divertor configurations.

In figure 3, the distance between the equilibrium α and the minimum α required for ballooning mode destabilization is plotted as a function of the edge pressure $p_{\rho=0.95}$, where $\rho = \sqrt{(\psi - \psi_{axis})/(\psi_{separatrix} - \psi_{axis})}$ is a normalized radius, and colored by applied power. The strong NT discharges cover a range of edge stability, with some degradation in edge pressure appearing at the highest P_{aux}. Importantly, no ELM-free discharges support larger gradients than allowed by ideal ballooning stability. This behavior shows that, while particular discharges in this dataset may be limited by additional physics mechanisms (potentially including electron temperature gradient modes [19, 35], kinetic ballooning modes [31], micro-tearing modes [36] and/or zonal flow screening [37]), the infinite-n ballooning mode sets an absolute upper limit on the pressure gradient in the NT edge. For comparison, a selection of strong ELMy H-mode discharges (from [17, 26]) are also shown in figure 3. In these cases, which require weak δ, the plasma is able to access the 2^{nd} stability region through additional growth of the density pedestal. The ELMy H-mode plasmas therefore achieve normalized gradients well above the 1^{st} stability limit that dominates behavior at strong NT. The inset of figure 3 shows a comparison of the pressure profiles for representative NT ELM-free and weak NT ELMy H-mode shots, as well as an L-mode profile from a PT discharge (from [5]), all at matched $P_{aux} = 8\,MW$. Though the H-mode case has the largest pedestal (even larger pedestals may be achieved in PT with $\delta \gtrsim 0.2$ [38], as seen in the RMP and QH-mode data presented below), the ELM-free NT edge still features a significantly enhanced edge pressure gradient compared to the more typical PT L-mode profile. This example also demonstrates that the strong NT edge does not limit total plasma performance, as the ELM-free NT edge enables higher pressure gradients throughout the core region despite a lower pedestal compared to H-mode. We note that, to remain in L-mode at $P_{aux} = 8\,MW$, the PT L-mode included in the inset of Figure 3 includes significant core radiation. Comparisons of PT L-mode profiles with NT profiles at matched lower power show similar (though slightly less

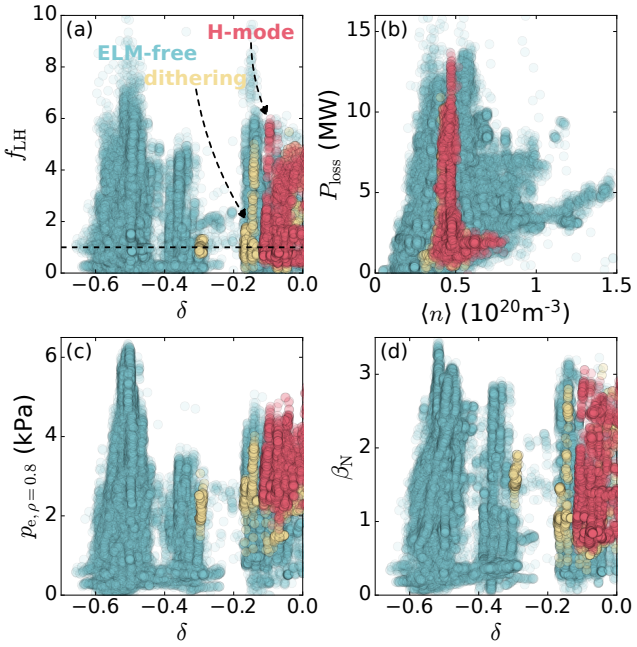

FIG. 4: (a) For the entire NT dataset on DIII-D, the H-mode threshold power fraction f_{LH} is shown as a function of δ. ELMy H-modes are colored in red, dithering periods in yellow, and ELM-free periods in blue. (b) The volume-averaged density $\langle n \rangle$ and separatrix power P_{loss} reveal the breadth of the ELM-free space. (c) The edge pressure (at $\rho = 0.8$) and (d) β_N show no degradation at strong $\delta < 0$, despite the suppression of ELMs.

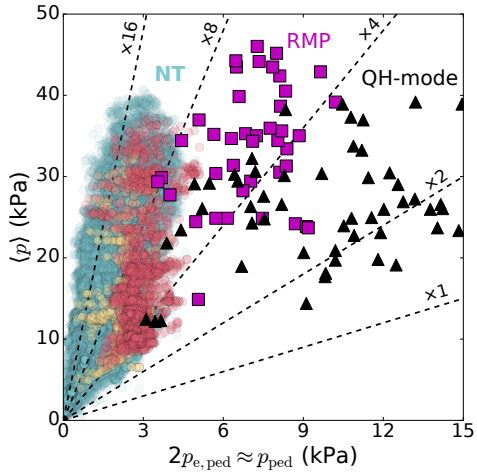

FIG. 5: The volume-averaged pressure $\langle p \rangle$ and pedestal pressure p_{ped} for ELM-free NT discharges (blue), PT RMP ELM-suppressed H-modes (magenta) and PT QH-modes (black) on DIII-D are compared. ELMy H-mode (red) and dithering regimes (yellow) at weak NT are also shown.

exaggerated) trends.

In figure 4, we further characterize the edge behavior by examining instantaneous time slices every 20 ms throughout 890 separate discharges (the entire DIII-D NT dataset, $\sim 85\%$ of which uses the new machine configuration). Figure 4(a) shows access to the NT ELM-free state as a function δ and H-mode threshold power fraction $f_{LH} = P_{loss}/P_{LH08}$, where

$$P_{loss} = P_{aux} + P_{Ohmic} - P_{rad,core} - \frac{dW_{MHD}}{dt} \quad (2)$$

is a measure of the power crossing the separatrix and

$$P_{LH08} = 0.0488\,\overline{n}^{0.717} B_t^{0.803} S^{0.941} \quad (3)$$

is the typical threshold power needed for H-mode access based on the scalings in reference [39]. Here the line-averaged plasma density $\overline{n}$ is given in [10^{20} m^{-3}], B_t in [T], and the plasma surface area S in [m^2]. The vast majority of this data resides at effective charges of $1.5 < Z_{eff} < 2.5$, though $\sim 2\%$ include significant intrinsic or seeded impurities with Z_{eff} up to 6. ELM-free operation is regularly achieved on DIII-D below a critical triangularity of $\delta_{crit} \sim -0.15$, and dithering regimes (from figure 2) only exist at $\delta \gtrsim -0.3$, even when heating the plasma with upwards of eight times the expected H-mode threshold power P_{LH08}. In figure 4(b), we show a traditional view of the L-to-H transition space expected for PT discharges by comparing the volume-averaged density to the total power crossing the separatrix (P_{loss}). It is readily observed that the ELM-free operating space occupies a broad parameter space, highlighting that ELM-suppression in NT is insensitive to control parameters and thus inherently different than in PT.

In addition to demonstrating robust ELM suppression across the entire operational space, figure 4(c) shows how the edge pressure p_e (measured at a normalized radius of $\rho = 0.8$) is impacted by the ELM-free NT edge. H-mode access predictably leads to enhanced p_e at small $|\delta|$, before the ideal ballooning physics takes effect at more pronounced NT. However, the lack of H-mode at stronger negative δ does not prevent the ELM-free scenarios from reaching or exceeding edge pressures achieved by H-modes in weaker shapes. Normalized measures of global performance tell a similar story over the DIII-D NT operational space, as shown in figure 4(d). Neither β_N nor H_{98y2} is hindered by the ELM suppression mechanisms of NT. Instead, as will be elaborated in future work, a large portion of the new DIII-D NT dataset meets reasonable reactor targets of $H_{98y2} > 1$, $\beta_N > 2.5$ and Greenwald fractions $f_{GW} > 1$ at triangularities of $\delta \sim -0.5$, reinforcing the exceptional NT performance previously reported in [16, 17, 40]. Indeed, the highest performing NT discharges achieved to date on DIII-D are completely ELM-free.

The high performance achieved by the ELM-free NT edge is also demonstrated in figure 5, which compares the volume-averaged pressures $\langle p \rangle$ and edge pressures $p_{ped} \approx 2 \times p_{e,ped}$ for the ELM-free NT dataset and the DIII-D RMP ELM-suppressed and QH-mode datasets (both in PT, from reference [5]). As expected, both the RMP and QH-mode discharges feature significantly larger pedestal pressures than the NT configurations due

to their H-mode characteristics. However, the maximum achievable $\langle p \rangle$ between all three regimes remains quite comparable, highlighting that the ELM-free NT edge does not inhibit steep profile gradients from forming in the core region where fusion power will be concentrated. So while the NT regime relieves physics risk from integration issues, it increases the burden on core confinement to achieve sufficiently high plasma performance despite lower $p_{\rm ped}$. We note here that many of the RMP and QH mode discharges included in figure 5 access an ELM-free regime for only a portion ($\lesssim 30\%$) of the full shot, while NT discharges included are entirely ELM free for the full discharge duration. This extremely robust nature of NT ELM avoidance is a unique and promising feature among potential ELM suppression techniques.

Finally, we would like to reiterate that the traditional relationship between L-mode and H-mode as established by decades of experience in PT does not apply to discharges with strong NT. Negative triangularity plasmas are *not* kept out of H-mode via a lack of power crossing the separatrix, as is typically assumed of L-mode plasmas in PT: no evidence of an LH transition threshold power in plasmas with strong enough NT shaping has yet been encountered. Further, ELM-free scenarios in NT can have pressure profile gradients (and resulting $E_{\rm r}$ shear) similar to those observed in ELMy H-mode scenarios at null or weakly negative triangularity. These plasmas occupy a unique space in the operational domain for tokamaks (naturally ELM-free operation at high normalized performance) and are held there regardless of plasma conditions due to a unique physical mechanism (gradient limiting via ideal ballooning modes in the plasma edge). As such, we refer to these plasmas not by "L-mode" as suggested by the current literature, but rather propose that they be categorized simply as having an ELM-free NT edge.

Acknowledgments. We would like to acknowledge the tremendous support of our colleagues at the DIII-D National Fusion Facility whose tireless efforts made this work possible. Part of data analysis for this work was performed using the OMFIT integrated modeling framework [41, 42]. This material was supported by the U.S. Department of Energy, Office of Science, Office of Fusion Energy Sciences, using the DIII-D National Fusion Facility, a DOE Office of Science user facility, under Awards DE-SC0022270, DE-SC0022272, DE-SC0020287, DE-FG02-97ER54415, DE-AC52-07NA27344 and DE-FC02-04ER54698. This report is prepared as an account of work sponsored by an agency of the United States Government. Neither the United States Government nor any agency thereof, nor any of their employees, makes any warranty, express or implied, or assumes any legal liability or responsibility for the accuracy, completeness, or usefulness of any information, apparatus, product, or process disclosed, or represents that its use would not infringe privately owned rights. Reference herein to any specific commercial product, process, or service by trade name, trademark, manufacturer, or otherwise, does not necessarily constitute or imply its endorsement, recommendation, or favoring by the United States Government or any agency thereof. The views and opinions of authors expressed herein do not necessarily state or reflect those of the United States Government or any agency thereof.

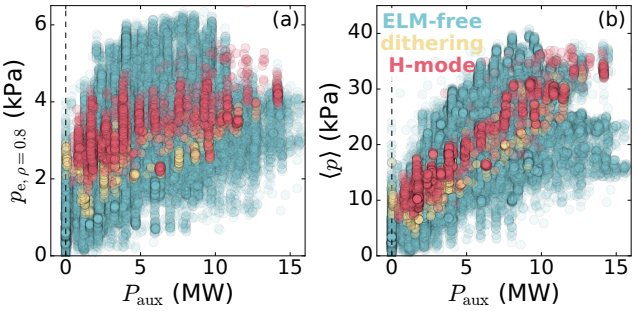

FIG. 6: For the entire NT dataset on DIII-D, (a) the edge pressure and (b) the volume-averaged pressure are plotted against auxiliary heating power.

Appendix on the role of heating power. — Another interesting question that can be asked of this dataset concerns the role of heating power in setting the edge phenomenology and the core performance in NT scenarios. To supplement the discussion of figure 4, which shows that access to the ELM-free state does not depend on heating power as long as $\delta < \delta_{\rm crit}$, figure 6 shows both $p_{{\rm e},\rho=0.8}$ and $\langle p \rangle$ as explicit functions of $P_{\rm aux}$. In both cases, the pressures attainable in the ELM-free NT state can match or even exceed those encountered in weak NT ($\delta > \delta_{\rm crit}$) ELMy H-modes at similar powers. This occurs as a result of the non-stiff nature of transport in the edge region ($\rho \gtrsim 0.8$) of NT plasmas, which allows for gradient growth in the NT edge even without accessing H-mode values [43]. Notably, this also holds at low power where H-modes typically exceed L-mode confinement.

Figure 6 also illustrates a potentially important advantage of NT configurations over PT H-modes in terms of reactor implementation. While PT H-mode reactor scenarios rely on maintaining a certain level of power ($\gtrsim P_{\rm LH08}$) crossing the separatrix to maintain good core confinement, NT plasmas are not subject to this power constraint. This favorable property of NT plasmas could potentially alleviate control issues encountered during the L-H plasma state bifurcation in PT, relax constraints placed on an auxiliary heating systems in a reactor environment, and allow for high edge pressures at low $P_{\rm sep}$ where the power exhaust problem is ameliorated.

[1] F. Wagner, G. Fussmann, T. Grave, M. Keilhacker, M. Kornherr, K. Lackner, K. Mccormick, E. R. Muller, A. Stabler, G. Becker, K. Bernhardi, U. Ditte, A. Eber-

hagen, O. Gehre, J. Gernhardt, G. V. Gierke, E. Glock, O. Gruber, G. Haas, M. Hesse, G. Janeschitz, F. Karger, S. Kissel, O. K1qber, G. Lisitano, H. M. Mayer, D. Meisel, V. Mertens, H. Murrnann, W. Poschenrieder, H. Rapp, H. Rohr, F. Ryter, F. Schneider, G. Siller, P. Smeulders, F. Soldner, E. Speth, K.-H. Steuer, Z. Szymanski, and O. Vollmer, Physical Review Letters **53**, 1453 (1984).

[2] H. Zohm, Plasma Physics and Controlled Fusion **38**, 105 (1996).

[3] A. W. Leonard, Physics of Plasmas **21**, 10.1063/1.4918359 (2014).

[4] J. P. Gunn, S. Carpentier-Chouchana, F. Escourbiac, T. Hirai, S. Panayotis, R. A. Pitts, Y. Corre, R. Dejarnac, M. Firdaouss, M. Kočan, M. Komm, A. Kukushkin, P. Languille, M. Missirlian, W. Zhao, and G. Zhong, Nuclear Fusion **57**, 10.1088/1741-4326/aa5e2a (2017).

[5] C. Paz-Soldan, Plasma Physics and Controlled Fusion **63**, 10.1088/1361-6587/ac048b (2021).

[6] K. H. Burrell, M. E. Austin, D. P. Brennan, J. C. DeBoo, E. J. Doyle, C. Fenzi, C. Fuchs, P. Gohil, C. M. Greenfield, R. J. Groebner, L. L. Lao, T. C. Luce, M. A. Makowski, G. R. McKee, R. A. Moyer, C. C. Petty, M. Porkolab, C. L. Rettig, T. L. Rhodes, J. G. Rost, B. W. Stallard, E. J. Strait, E. J. Synakowski, M. R. Wade, J. G. Watkins, and W. P. West, Physics of Plasmas **8**, 2153 (2001).

[7] W. Suttrop, A. Kirk, V. Bobkov, M. Cavedon, M. Dunne, R. McDermott, H. Meyer, R. Nazikian, C. Paz-Soldan, D. Ryan, E. Viezzer, M. Willensdorfer, The ASDEX Upgrade, and MST1 Teams, Nuclear Fusion **58**, 096031 (2018).

[8] M. Faitsch, T. Eich, G. Harrer, E. Wolfrum, D. Brida, P. David, M. Dunne, L. Gil, B. Labit, and U. Stroth, Nuclear Fusion **63**, 10.1088/1741-4326/acd464 (2023).

[9] D. G. Whyte, A. E. Hubbard, J. W. Hughes, B. Lipschultz, J. E. Rice, E. S. Marmar, M. Greenwald, I. Cziegler, A. Dominguez, T. Golfinopoulos, N. Howard, L. Lin, R. M. McDermottb, M. Porkolab, M. L. Reinke, J. Terry, N. Tsujii, S. Wolfe, S. Wukitch, and Y. Lin, Nuclear Fusion **50**, 10.1088/0029-5515/50/10/105005 (2010).

[10] S. Frank, C. J. Perks, A. O. Nelson, T. Qian, S. Jin, A. J. Cavallaro, A. Rutkowski, A. H. Reiman, J. P. Freidberg, P. Rodriguez-Fernandez, and D. G. Whyte, Nuclear Fusion **62**, 10.1088/1741-4326/ac95ac (2022).

[11] M. Greenwald, R. Boivin, P. Bonoli, R. Budny, C. Fiore, J. Goetz, R. Granetz, A. Hubbard, I. Hutchinson, J. Irby, B. Labombard, Y. Lin, B. Lipschultz, E. Marmar, A. Mazurenko, D. Mossessian, T. Sunn Pedersen, C. S. Pitcher, M. Porkolab, J. Rice, W. Rowan, J. Snipes, G. Schilling, Y. Takase, J. Terry, S. Wolfe, J. Weaver, B. Welch, and S. Wukitch, Physics of Plasmas **6.5**, 1943 (1999).

[12] E. Viezzer, M. Austin, M. Bernert, K. Burrell, P. Cano-Megias, X. Chen, D. Cruz-Zabala, S. Coda, M. Faitsch, O. Février, L. Gil, C. Giroud, T. Happel, G. Harrer, A. Hubbard, J. Hughes, A. Kallenbach, B. Labit, A. Merle, H. Meyer, C. Paz-Soldan, P. Oyola, O. Sauter, M. Siccinio, D. Silvagni, and E. Solano, Nuclear Materials and Energy **34**, 10.1016/j.nme.2022.101308 (2023).

[13] A. Pochelon, T. Goodman, M. Henderson, C. Angioni, R. Behn, S. Coda, F. Hofmann, J.-P. Hogge, N. Kirneva, A. Martynov, J.-M. Moret, Z. Pietrzyk, F. Porcelli, H. Reimerdes, J. Rommers, E. Rossi, O. Sauter, M. Tran, H. Weisen, S. Alberti, S. Barry, P. Blanchard, P. Bosshard, R. Chavan, B. Duval, Y. Esipchuck, D. Fasel, A. Favre, S. Franke, I. Furno, P. Gorgerat, P.-F. Isoz, B. Joye, J. Lister, X. Llobet, J.-C. Magnin, P. Mandrin, A. Manini, B. Marlétaz, P. Marmillod, Y. Martin, J.-M. Mayor, J. Mlynar, C. Nieswand, P. Paris, A. Perez, R. Pitts, K. Razumova, A. Refke, E. Scavino, A. Sushkov, G. Tonetti, F. Troyon, W. V. Toledo, and P. Vyas, Nuclear Fusion **39**, 1807 (1999).

[14] Y. Camenen, A. Pochelon, R. Behn, A. Bottino, A. Bortolon, S. Coda, A. Karpushov, O. Sauter, and G. Zhuang, Nuclear Fusion **47**, 510 (2007).

[15] S. Coda, A. Merle, O. Sauter, L. Porte, F. Bagnato, J. Boedo, T. Bolzonella, O. Février, B. Labit, A. Marinoni, A. Pau, L. Pigatto, U. Sheikh, C. Tsui, M. Vallar, and T. Vu, Plasma Physics and Controlled Fusion **64**, 10.1088/1361-6587/ac3fec (2022).

[16] M. E. Austin, A. Marinoni, M. L. Walker, M. W. Brookman, J. S. Degrassie, A. W. Hyatt, G. R. McKee, C. C. Petty, T. L. Rhodes, S. P. Smith, C. Sung, K. E. Thome, and A. D. Turnbull, Physical Review Letters **122**, 10.1103/PhysRevLett.122.115001 (2019).

[17] A. Marinoni, M. Austin, A. Hyatt, S. Saarelma, F. Scotti, Z. Yan, C. Chrystal, S. Coda, F. Glass, J. Hanson, A. McLean, D. Pace, C. Paz-Soldan, C. Petty, M. Porkolab, L. Schmitz, F. Sciortino, S. Smith, K. Thome, F. Turco, and the DIII-D Team, Nuclear Fusion **61**, 10.1088/1741-4326/ac1f60 (2021).

[18] T. Happel, T. Pütterich, D. Told, M. G. Dunne, R. Fischer, J. Hobirk, R. M. McDermott, U. Plank, and T. ASDEX Upgrade Team, Nuclear Fusion **63**, 10.1088/1741-4326/ac8563 (2022).

[19] A. Marinoni, O. Sauter, and S. Coda, Reviews of Modern Plasma Physics **5**, 6 (2021).

[20] ITER Physics Expert Group on Confinement and Transport, Nuclear Fusion **39** (1999).

[21] S. Y. Medvedev, M. Kikuchi, L. Villard, T. Takizuka, P. Diamond, H. Zushi, K. Nagasaki, X. Duan, Y. Wu, A. A. Ivanov, A. A. Martynov, Y. Y. Poshekhonov, A. Fasoli, and O. Sauter, Nuclear Fusion **55**, 10.1088/0029-5515/55/6/063013 (2015).

[22] M. Kikuchi, T. Takizuka, S. Medvedev, T. Ando, D. Chen, J. X. Li, M. Austin, O. Sauter, L. Villard, A. Merle, M. Fontana, Y. Kishimoto, and K. Imadera, Nuclear Fusion **59**, 10.1088/1741-4326/ab076d (2019).

[23] A. O. Nelson, A. W. Hyatt, W. P. Wehner, A. S. Welander, C. Paz-Soldan, T. H. Osborne, H. Anand, and K. E. Thome, Plasma Physics and Controlled Fusion **65**, 10.1088/1361-6587/acbe65 (2023).

[24] A. O. Nelson, C. Paz-Soldan, and S. Saarelma, Nuclear Fusion **62**, 10.1088/1741-4326/ac8064 (2022).

[25] R. Fitzpatrick and A. O. Nelson, Physics of Plasmas **27**, 10.1063/5.0011738 (2020).

[26] S. Saarelma, M. E. Austin, M. Knolker, A. Marinoni, C. Paz-Soldan, L. Schmitz, and P. B. Snyder, Plasma Physics and Controlled Fusion **63**, 10.1088/1361 (2021).

[27] C. Bishop, Nuclear Fusion **26**, 1063 (1986).

[28] R. L. Miller, Y. R. Lin-Liu, A. D. Turnbull, V. S. Chan, L. D. Pearlstein, O. Sauter, and L. Villard, Physics of Plasmas **4**, 1062 (1997).

[29] P. B. Snyder, H. R. Wilson, J. R. Ferron, L. L. Lao, A. W. Leonard, T. H. Osborne, A. D. Turnbull, D. Mossessian, M. Murakami, and X. Q. Xu, Physics of Plasmas **9**, 2037

(2002).
[30] L. Radovanovic, M. Dunne, E. Wolfrum, G. Harrer, M. Faitsch, R. Fischer, and F. Aumayr, Nuclear Fusion **62**, 10.1088/1741-4326/ac6d6a (2022).
[31] A. Merle, O. Sauter, and S. Yu Medvedev, Plasma Physics and Controlled Fusion **59**, 10.1088/1361-6587/aa7ac0 (2017), publisher: Institute of Physics Publishing.
[32] S. Y. Medvedev, A. A. Ivanov, A. A. Martynov, Y. Y. Poshekhonov, R. Behn, Y. R. Martin, A. Pochelon, O. Sauter, and L. Villard, 35th EPS Conference on Plasma Physics **32D**, 1.072 (2008).
[33] A. Pochelon, P. Angelino, R. Behn, S. Brunner, S. Coda, N. Kirneva, S. Y. Medvedev, H. Reimerdes, J. Rossel, O. Sauter, L. Villard, D. Wagńer, A. Bottino, Y. Camenen, G. P. Canal, P. K. Chattopadhyay, B. P. Duval, A. Fasoli, T. P. Goodman, S. Jolliet, A. Karpushov, B. Labit, A. Marinoni, J. M. Moret, A. Pitzschke, L. Porte, M. Rancic, and V. S. Udintsev, Plasma and Fusion Research **7**, 10.1585/pfr.7.2502148 (2012).
[34] Z. Xing, D. Eldon, A. O. Nelson, M. A. Roelofs, W. J. Eggert, O. Izacard, A. Glasser, N. Logan, O. Meneghini, S. P. Smith, R. Nazikian, and E. Kolemen, Fusion Engineering and Design **163**, 112163 (2021).
[35] G. Merlo, S. Brunner, O. Sauter, Y. Camenen, T. Görler, F. Jenko, A. Marinoni, D. Told, and L. Villard, Plasma Physics and Controlled Fusion **57**, 10.1088/0741-3335/57/5/054010 (2015).
[36] A. O. Nelson, F. M. Laggner, A. Diallo, D. R. Smith, Z. A. Xing, R. Shousha, and E. Kolemen, Nuclear Fusion **61**, 116083 (2021).
[37] R. Singh and P. H. Diamond, Nuclear Fusion **62**, 10.1088/1741-4326/ac945e (2022).
[38] A. O. Nelson, F. M. Laggner, R. J. Groebner, B. A. Grierson, O. Izacard, D. Eldon, M. Shafer, A. W. Leonard, D. Shiraki, A. C. Sontag, and E. Kolemen, Nuclear Fusion **60**, 10.1088/1741-4326/ab5e65 (2020).
[39] Y. R. Martin and T. Takizuka, Journal of Physics: Conference Series **123**, 10.1088/1742-6596/123/1/012033 (2008).
[40] A. Marinoni, M. E. Austin, A. W. Hyatt, M. L. Walker, J. Candy, C. Chrystal, C. J. Lasnier, G. R. McKee, T. Odstrčil, C. C. Petty, M. Porkolab, J. C. Rost, O. Sauter, S. P. Smith, G. M. Staebler, C. Sung, K. E. Thome, A. D. Turnbull, and L. Zeng, Physics of Plasmas **26**, 10.1063/1.5091802 (2019).
[41] O. Meneghini, S. P. Smith, L. L. Lao, O. Izacard, Q. Ren, J. M. Park, J. Candy, Z. Wang, C. J. Luna, V. A. Izzo, B. A. Grierson, P. B. Snyder, C. Holland, J. Penna, G. Lu, P. Raum, A. McCubbin, D. M. Orlov, E. A. Belli, N. M. Ferraro, R. Prater, T. H. Osborne, A. D. Turnbull, and G. M. Staebler, Nuclear Fusion **55**, 10.1088/0029-5515/55/8/083008 (2015).
[42] N. C. Logan, B. A. Grierson, S. R. Haskey, S. P. Smith, O. Meneghini, and D. Eldon, Fusion Science and Technology **74**, 125 (2018).
[43] O. Sauter, S. Brunner, D. Kim, G. Merlo, R. Behn, Y. Camenen, S. Coda, B. P. Duval, L. Federspiel, T. P. Goodman, A. Karpushov, A. Merle, and T. Team, Physics of Plasmas **21**, 10.1063/1.4876612 (2014).